Growth and Characterization of Metal(II) Alkanebisphosphonate Multilayer Thin Films on Gold Surfaces

Huey C. Yang, Katsunori Aoki, Hun-Gi Hong, Debra D. Sackett, Mark F. Arendt, Shueh-Lin Yau, Christine M. Bell, and Thomas E. Mallouk*,†

Contribution from the Department of Chemistry and Biochemistry, The University of Texas at Austin, Austin, Texas 78712

Received July 29, 1993®

Abstract: Thin films of divalent metal (Zn and Cu) alkanebisphosphonates grow on gold surfaces modified with (4-mercaptobutyl)phosphonic acid by alternate immersion in 5 mM ethanolic solutions of the metal acetate or perchlorate salt and $H_2O_3P(CH_2)_nPO_3H_2$, $n = 8$, 10, 12, and 14. Growth of each layer is remarkably fast. Well-ordered multilayers can be deposited with 10-min adsorption steps, and films of 100-layer thickness are easily prepared. Quartz crystal microbalance (QCM) measurements of mass changes are in quantitative agreement with adsorption of individual layers corresponding to bulk stoichiometry ($M_2[O_3P(CH_2)_nPO_3]\cdot 2H_2O$) and packing density. Ellipsometric film thicknesses agree closely with measured layer spacings from X-ray diffraction of bulk solids, and alkyl chain tilt angles (31°) for the Zn films are essentially the same as predicted from the crystal structure of $Fe(O_3PC_2H_5)\cdot H_2O$. Reflectance infrared spectra show that the alkyl chains are less ordered in the films than in the bulk solids for $M_2[O_3P(CH_2)_nPO_3]\cdot 2H_2O$, $n = 8$, but that they are well-ordered for $n = 14$. Atomic force microscopy (AFM) images of multilayer films show that they follow the surface topology of the underlying gold and that they can be mechanically removed from the substrate. The depth of etch pits prepared with the AFM tip matches the film thickness measured by ellipsometry.

The preparation, characterization, and reactivity of monolayer and multilayer organic thin films are of significant current interest in materials chemistry.[1] Apart from providing an avenue to predictable surface physical properties such as wettability[2] and tribology,[3] ultrathin films create a structurally tailored and chemically well-defined vehicle for surface reactions. They are therefore of interest in the study of a variety of chemical phenomena, which include catalysis,[4] electron-transfer reactions,[5] passivation of semiconductor surfaces,[6] and corrosion inhibition.[7]

One of the most effective methods for producing compact monolayers is through the self-assembly process, in which a reactive group at one end of the molecule (usually a carboxylate, reactive silane, or thiol) chemisorbs or binds covalently to the surface, and noncovalent intermolecular forces lead to in-plane ordering. The structure and chemistry of monolayers formed by adsorbing such molecules either from solution[1] or from the vapor phase[8] has now been quite extensively studied. By comparison, the techniques for preparing well-ordered *multilayer* thin films by self-assembly methods are much less highly developed. Although the synthesis and characterization of organic multilayer assemblies is generally more challenging than that of monolayers, such films offer the promise of amplification of the properties of a single layer, for example in optical second-harmonic generation (SHG).[9] Also, if one prepares films in which chemically different layers can be juxtaposed to form heterostructures, then in principle rather intricate device functions, which are needed in such areas as artificial photosynthesis, molecular electronics, chemical sensing, and separations, might be attained.

To date, several different procedures have been developed for interconnecting self-assembling monolayers in the third dimension.[10] These include the sequential adsorption–chemical activation strategy first described by Netzer and Sagiv[11] and further developed by Tilman et al.,[12] as well as newer methods based on ionic[13] and coordinate covalent[14] interlayer connections. One of the most successfully applied of these techniques involves

† Current address: Department of Chemistry, Pennsylvania State University, University Park, PA 16802.

® Abstract published in *Advance ACS Abstracts*, November 15, 1993.

(1) Ulman, A. *An Introduction to Ultrathin Organic Films: From Langmuir–Blodgett to Self-Assembly*; Harcourt Brace Jovanovich: Boston, 1991.

(2) (a) Bain, C. D.; Whitesides, G. M. *Angew. Chem., Intl. Ed. Engl.* **1989**, *28*, 506. (b) Whitesides, G. M.; Laibinis, P. E. *Langmuir* **1990**, *6*, 87. (c) Laibinis, P. E.; Whitesides, G. M. *J. Am. Chem. Soc.* **1992**, *114*, 1990. (d) Chaudhury, M. K.; Whitesides, G. M. *Science* **1992**, *256*, 1539.

(3) Overney, R. M.; Meyer, E.; Frommer, J.; Brodbeck, D.; Lüthi, R.; Howald, L.; Güntherodt, H.-J.; Fujihira, M.; Takano, H.; Gotoh, Y. *Nature* **1992**, *359*, 133.

(4) Somorjai, G. A. *Chemistry in Two Dimensions: Surfaces*; Cornell University Press: Ithaca, NY, 1981.

(5) (a) Chidsey, C. E. D.; Bertozzi, C. R.; Putvinski, T. M.; Mujsce, A. M. *J. Am. Chem. Soc.* **1990**, *112*, 4301. (b) Chidsey, C. E. D. *Science* **1991**, *251*, 919. (c) Porter, M. D.; Bright, T. B.; Allara, D. L.; Chidsey, C. E. D. *J. Am. Chem. Soc.* **1987**, *109*, 3559. (d) Miller, C. M.; Majda, M. *J. Am. Chem. Soc.* **1986**, *108*, 3118. (e) Miller, C.; Cuendet, P.; Gratzel, M. *J. Phys. Chem.* **1991**, *95*, 877. (f) Miller, C.; Gratzel, M. *J. Phys. Chem.* **1991**, *95*, 5225. (g) Kuhn, H. *Pure Appl. Chem.* **1979**, *51*, 341. (h) Finklea, H. O.; Hanshaw, D. D. *J. Am. Chem. Soc.* **1992**, *114*, 3173. (i) Finklea, H. O.; Avery, S.; Lynch, M.; Turtsch, T. *Langmuir* **1987**, *3*, 409. (j) Finklea, H. O.; Robinson, L. R.; Blackburn, A.; Richter, B.; Allara, D.; Bright, T. *Langmuir* **1986**, *2*, 239. (k) Li, T. T.-T.; Weaver, M. J. *J. Am. Chem. Soc.* **1984**, *106*, 6107. (l) Li, T. T.-T.; Liu, H. Y.; Weaver, M. J. *J. Am. Chem. Soc.* **1984**, *106*, 1233. (m) Li, T. T.-T.; Weaver, M. J. *J. Electroanal. Chem.* **1985**, *188*, 121. (n) Weaver, M. J.; Li, T. T.-T. *J. Phys. Chem.* **1986**, *90*, 3823.

(6) (a) Roberts, G. G. *Adv. Phys.* **1985**, *34*, 475. (b) Swalen, J. D.; Allara, D. L.; Andrade, J. D.; Chandross, E. A.; Garoff, S.; Israelachvili, J.; McCarthy, T. J.; Murray, R.; Pease, R. F.; Rabolt, J. F.; Wynne, K. J.; Yu, H. *Langmuir* **1987**, *3*, 932. (c) Larkins, G. L., Jr.; Fung, C. D.; Rickert, S. E. *Thin Solid Films* **1989**, *180*, 217. (d) Tabib-Azar, M.; Dewa, A. S.; Ho, W. H. *Appl. Phys. Lett.* **1988**, *52*, 206.

(7) Noyota, T.; Poling, G. W. *Corrosion* **1979**, *35*, 193.

(8) Sun, L.; Thomas, R. C.; Crooks, R. M.; Ricco, A. J. *J. Am. Chem. Soc.* **1991**, *113*, 8550.

(9) (a) Popovitz-Biro, R.; Hill, K.; Hung, D. J.; Lahav, M.; Leiserowitz, L.; Sagiv, J.; Hsiung, H.; Meredith, G. R.; Vanherzeele, H. *J. Am. Chem. Soc.* **1990**, *112*, 2498. (b) Li, D.; Ratner, M. A.; Marks, T. J.; Zhang, C. H.; Yang, J.; Wong, G. K. *J. Am. Chem. Soc.* **1990**, *112*, 7389. (c) Katz, H. E.; Scheller, G.; Putvinski, T. M.; Schilling, M. L.; Wilson, W. L.; Chidsey, C. E. D. *Science* **1991**, *254*, 1485.

(10) We confine our discussion here to multilayers produced by self-assembly from solution. For reviews of monolayer transfer (Langmuir–Blodgett methods) see, e.g.: (a) Gaines, G. L., Jr. *Insoluble Monolayers at Liquid-Gas Interfaces*; Wiley: New York, 1966. (b) Agarwal, V. K. *Phys. Today* **1988**, June, 40.

(11) (a) Netzer, L.; Sagiv, J. *J. Am. Chem. Soc.* **1983**, *105*, 674. (b) Moaz, R.; Netzer, L.; Gun, J.; Sagiv, J. *J. Chim. Phys. Phys.-Chim. Biol.* **1988**, *85*, 1059.

(12) (a) Tilman, A.; Ulman, A.; Penner, T. L. *Langmuir* **1989**, *5*, 101.

(13) (a) Lee, H.; Kepley, L. J.; Hong, H.-G.; Mallouk, T. E. *J. Am. Chem. Soc.* **1988**, *110*, 618. (b) Lee, H.; Kepley, L. J.; Hong, H.-G.; Akhter, S.; Mallouk, T. E. *J. Phys. Chem.* **1988**, *92*, 2597. (c) Cao, G.; Hong, H.-G.; Mallouk, T. E. *Acc. Chem. Res.* **1992**, *25*, 420. (d) Akhter, S.; Lee, H.; Hong, H.-G.; Mallouk, T. E.; White, J. M. *J. Vac. Sci. Technol., A* **1989**, *7*, 1608. (e) Evans, S. D.; Ulman, A.; Goppert-Berarducci, K. E.; Gerenser, L. J. *J. Am. Chem. Soc.* **1991**, *113*, 5866. (f) Decher, G.; Hong, J. D.; Schmitt, J. *Thin Solid Films* **1992**, *210/211*, 831.

0002-7863/93/1515-11855$04.00/0

sequential adsorption of the components of tetravalent metal phosphonate salts from aqueous and nonaqueous solutions.[13a-d,15,16] Films produced in this way are structurally analogous to layered metal–organic compounds, in which the metal–oxygen–phosphorus network, held together by strong ionic and covalent bonds, directs the juxtaposition of interlamellar organic groups.

While the tetravalent metal phosphonates are the best known of these materials,[17] quite a few layered phosphonate salts of di- and trivalent elements have been recently described.[18] Some of these materials undergo interesting reactions, such as shape-selective intercalation at "templated" binding salts,[19] which are unknown in the tetravalent metal salts. Moreover, salts of the di- and trivalent metals tend to be less insoluble than their tetravalent counterparts and so tend to precipitate from solution with a higher degree of crystallinity.

In this paper we report the growth of divalent metal phosphonate multilayer thin films and compare their properties to films of zirconium phosphonates. Growth of the divalent (Zn^{II}, Cu^{II}) metal films is remarkably fast, compared to those of Zr^{IV}, so that rather thick films (up to 100 layers) are easily prepared by sequential dipping/rinsing reactions at room temperature in ethanol. This property is important for potential applications such as growth of polar films for SHG, where relatively thick but highly ordered layers are required. Surface-sensitive probes establish that the divalent metal phosphonate films are well-ordered and that their stoichiometry and structure are very similar to those of the bulk $M_2(O_3P(CH_2)_nPO_3)\cdot 2H_2O$ salts.

Experimental Section

Materials. Bisphosphonic acids, $H_2O_3P(CH_2)_nPO_3H_2$ (abbreviated C_nBPA) were prepared by the Michaelis–Arbuzov reaction of $Br(CH_2)_nBr$ (n = 4, 8, 10, 12, 14; obtained from Karl Industries Inc.) with triethyl phosphite. $Br(CH_2)_nBr$ (20 mmol) and $P(OC_2H_5)_3$ (50 mmol) were refluxed at 150 °C for 6 h, the solution was cooled to room temperature, and about 30 mL of concentrated (36.5–38.0%) aqueous HCl solution was added. Heating was resumed at 100 °C overnight (16 h). The solution was cooled to room temperature, 10 mL of water was added, and the aqueous layer was then separated. The aqueous phase was evaporated in air at room temperature for ca. 2 days, and the white precipitate of C_nBPA was washed several times with HPLC grade CH_3CN and dried in vacuum.

Gold (99.999%) was sputtered onto glass slides (for IR, borosilicate glass, 25 × 25 mm) and silicon wafers (for ellipsometry, XPS and AFM, n-type (100), 10 × 10 mm), in a MRC (Materials Research Corporation, Orangeburg, NY) Model 8620 sputtering system at 10^{-2} Torr, with an rf power of 150 W and rf peak-to-peak voltage of 1.8 kV. The glass slides were cleaned prior to gold deposition in a fresh mixture of hot 1:3 v/v H_2O_2 (30%):H_2SO_4 (96%) for 30 min, rinsed with water followed by ethanol, dried in an oven at 140 °C overnight, and then subjected to 2 min of argon plasma etching prior to sputtering. The glass was primed with a 50-Å Cr layer followed by a 2000-Å Au layer. Silicon wafers were cleaned twice in trichloroethylene in an ultrasonic bath for 5 min and then twice in 2-propanol for 10 min and dried in a stream of dry nitrogen.

AT-cut gold-coated quartz crystal microbalance samples (QCM, Kyushu Dentsu Company, Ltd., Omura-city, Nagasaki, Japan) were cleaned prior to adsorption of the anchoring agent, (4-mercaptobutyl)-phosphonic acid (MBPA),[20] in hot chromic acid (saturated K_2CrO_4 in 90% H_2SO_4) for a few seconds and rinsed with copious amounts of water. The crystals, which had been polished on both sides by the manufacturer, had resonant frequencies of 6 and 9 MHz and a gold-coated (active) area of 2 × 0.159 cm^2. The surface roughness of the gold on the QCMs was determined electrochemically.[21] In this method, cyclic voltammetry was carried out in 0.1 M H_2SO_4 at a scan rate of 100 mV/s. The cyclic scan was initiated in the positive direction, with an anodic switching limit of +1.5 V vs SCE. The charge transferred to adsorbed oxygen atoms was estimated from the area under the cathodic gold oxide reduction peak. The roughness factor was then determined as the ratio of the measured charge to 482 $\mu C/cm^2$, which is the charge associated with monolayer coverage of adsorbed oxygen.[21a] For both the 6- and 9-MHz QCM samples, a roughness factor of 2.0 ± 0.2 was found.

Instrumentation and Measurements. Ellipsometric measurements were made with a Rudolf 437 ellipsometer as described previously[13b] except that an analyzing wavelength of 4880 Å was used. Ellipsometric parameters were measured following each bisphosphonic acid adsorption step. Gold-on-glass substrates were dried in a nitrogen stream prior to the measurements. The film thicknesses of the Zn_2-C_nBP multilayers were calculated from Δ and Ψ, using the gold refractive index, n_s = (1.119 ± 0.002) − (1.750 ± 0.100)i, determined from a blank sample. The experimental refractive index for gold was in agreement with literature data.[22] The refractive index of Zn_2-C_nBP, n_f = 1.540 − 0.000i, was estimated by the immersion method as follows: Zn_2-C_nBP (15 mg) was mixed individually with 2 mL of chloroform, benzene, anisole, benzyl alcohol, benzaldehyde, bromobenzene, and aniline. None of these solvents dissolve Zn_2-C_nBP. Only the benzyl alcohol (n_d = 1.538) and benzaldehyde (n_d = 1.544) gave apparently clear suspensions in which the bisphosphonate powder and solvent could barely be distinguished. The real part of the refractive index of the film, n_f, was therefore estimated to be 1.540. The imaginary part was assumed to be 0, and small variations in it (±0.01) had little effect on the film thickness calculations. A series of curves of Δ and Ψ were simulated by varying n_f from 1.538 to 1.544 and showed negligible differences.

Infrared spectra were recorded on a Nicolet 730 FTIR at 4-cm^{-1} resolution. The spectra were recorded in reflectance mode operating at an approximately 84° angle of incidence and with averaging of 2000 scans. The bulk samples were measured in a KBr pellet at the same resolution and with averaging of 300 scans. Details of the reflectance FTIR technique are described elsewhere.[23]

An AT-cut gold-coated QCM and a home-built oscillator circuit designed to drive the quartz crystal at its resonant frequency were employed for frequency measurements. The QCM was driven by a 5-V dc power supply, and the frequency of the vibrating quartz was measured with a Philips PM 6654C programmable high-resolution counter (Fluke Technical Center, Rockville, MD) connected to a microcomputer. In the experiment in which the formation of a Zn_2-C_nBP film on a QCM was monitored, a C_nBPA solution (5 mM in ethanol) was brought into the QCM unit for a defined period. The solution was removed from the system, and the crystal was rinsed with ethanol and then dried in air and the frequency measured. This procedure was repeated if a longer exposure

(14) (a) Bell, C. M.; Keller, S. W.; Mallouk, T. E. *Mater. Chem. Phys.* **1993**, *35*, 225. (b) Ham, W. K.; Zeppenfeld, A.; Page, C. J. Submitted for publication.

(15) (a) Putvinski, T. M.; Schilling, M. L.; Katz, H. E.; Chidsey, C. E. D.; Mujsce, A. M.; Emerson, A. B. *Langmuir* **1990**, *6*, 1567. (b) Katz, H. E.; Schilling, M. L.; Chidsey, C. E. D.; Putvinski, T. M.; Hutton, R. S. *Chem. Mater.* **1991**, *3*, 699.

(16) (a) Umemura, Y.; Tanaka, K.-I.; Yamagishi, A. *J. Chem. Soc., Chem. Commun.* **1992**, 67. (b) Byrd, H.; Pike, J. K.; Talham, D. R. *Chem. Mater.* **1993**, *5*, 709.

(17) (a) Alberti, G.; Costantino, U.; Allulli, S.; Tomassini, N. *J. Inorg. Nucl. Chem.* **1978**, *40*, 1113. (b) Alberti, G.; Costantino, U.; Giulietti, R. *J. Inorg. Nucl. Chem.* **1980**, *42*, 1062. (c) Clearfield, A. *Comments Inorg. Chem.* **1990**, *10*, 89 and references therein. (d) Dines, M. B.; DiGiacomo, P. *Inorg. Chem.* **1981**, *20*, 92. (e) Dines, M. B.; DiGiacomo, P.; Callahan, K. P.; Griffith, P. C.; Lane, R.; Cooksey, R. E. In *Chemically Modified Surfaces in Catalysis and Electrocatalysis*; Miller, J., Ed.; ACS Symposium Series 192; American Chemical Society: Washington, DC, 1982, p 223. (f) Alberti, G.; Costantino, U.; Kõrnyei, J.; Giovagnotti, M. L. L. *React. Polym.* **1985**, *4*, 1.

(18) (a) Cunningham, D.; Hennelly, P. J. D. *Inorg. Chim. Acta* **1979**, *37*, 95. (b) Cao, G.; Lynch, V. M.; Swinnea, J. S.; Mallouk, T. E. *Inorg. Chem.* **1990**, *29*, 2112. (c) Cao, G.; Lee, H.; Lynch, V. M.; Mallouk, T. E. *Inorg. Chem.* **1988**, *27*, 2781. (d) Cao, G.; Lee, H.; Lynch, V. M.; Mallouk, T. E. *Solid State Ionics* **1988**, *26*, 63. (e) Martin, K.; Squattrito, P. J.; Clearfield, A. *Inorg. Chim. Acta* **1989**, *155*, 7. (f) Johnson, J. W.; Jacobson, A. J.; Brody, J. F.; Lewandowski, J. T. *Inorg. Chem.* **1984**, *23*, 3842. (h) Huan, G.; Jacobson, A. J.; Johnson, J. W.; Corcoran, E. W., Jr. *Chem. Mater.* **1990**, *2*, 91. (i) Bujoli, B.; Palvadeau, P.; Rouxel, J. *Chem. Mater.* **1990**, *2*, 582. (j) Shieh, M.; Martin, K. J.; Squattrito, P. J.; Clearfield, A. *Inorg. Chem.* **1990**, *29*, 958. (k) Wang, R.-C.; Zhang, Y.-P.; Hu, H.; Frausto, R.; Clearfield, A. *Chem. Mater.* **1992**, *4*, 864. (l) Bujoli, B.; Pena, O.; Palvadeau, P.; Le Bideau, J.; Payen, C.; Rouxel, J. *Chem. Mater.* **1993**, *5*, 583.

(19) (a) Johnson, J. W.; Jacobson, A. J.; Butler, W. M.; Rosenthal, S. E.; Brody, J. F.; Lewandowski, J. T. *J. Am. Chem. Soc.* **1989**, *111*, 381. (b) Cao, G.; Mallouk, T. E. *Inorg. Chem.* **1991**, *30*, 1434. (c) Frink, K. J.; Wang, R.-C.; Colon, J. L.; Clearfield, A. *Inorg. Chem.* **1991**, *30*, 1438. (d) Zhang, Y.; Scott, K. J.; Clearfield, A. *Chem. Mater.* **1993**, *5*, 495.

(20) Hong, H-G.; Mallouk, T. E. *Langmuir* **1991**, *7*, 2362.

(21) (a) Oesch, U.; Janata, J. *Electrochim. Acta* **1983**, *28*, 1237. (b) Weber, J.; Samec, Z.; Maracek, V. *J. Electroanal. Chem.* **1978**, *89*, 271. (c) Burke, L. D.; McRann, M. *J. Electroanal. Chem.* **1981**, *125*, 387.

(22) Ordal, M. A.; Long, L. L.; Bell, R. J.; Bell, S. E.; Bell, R. R.; Alexander, R. W., Jr.; Ward, C. A. *Appl. Opt.* **1983**, *22*, 1099.

(23) Yang, H. C.; Magnera, T. F.; Lee, C.-M.; Bard, A. J.; Michl, J. *Langmuir* **1992**, *8*, 2740.

(24) (a) Abraham, F. F.; Batra, I. P. *Surf. Sci.* **1989**, *209*, L215. (b) Sugawara, Y.; Ishizaka, T.; Morita, S. *J. Vac. Sci. Technol.* **1991**, *B9*, 1092.

was needed for complete assembly of the monolayer. In these experiments the crystal was never disconnected from the measuring system, in order to avoid spurious frequency shifts.

X-ray powder diffraction patterns were obtained with an automated Model APO 3520 Philips powder diffractometer fitted with a graphite monochromator and a θ compensating slit (λ(Cu Kα) = 1.5478 Å). This arrangement permitted diffraction lines to be measured down to $2\theta = 1°$, with a precision of about ±0.02°.

X-ray photoelectron spectroscopy (XPS) analysis was performed in a Vacuum Generator ESCALAB MARK I (Mg Kα source, 330 W, 50 eV pass energy). Binding energies were calculated as the centroid of the respective peaks. The relative elemental ratios in the XPS sampling volume were determined from their relative peak areas and the VG elemental sensitivity factors.

Atomic force microscopy (AFM) was performed with a Nanoscope II, which operates by means of an optical deflection detection system. The tips and the cantilevers were made from microfabricated silicon nitride. The cantilevers had a "V" shape, with two 100-μm-long and 10-μm-wide legs; the force constants for the cantilevers varied between 0.1 and 0.5 N/cm. Red light from a semiconductor laser was focused onto the very end of the cantilever. As the cantilever moves up and down, the laser beam is deflected onto a two-segment photodetector and the signal is amplified. Apparent atomic resolution was attained when imaging atomically flat samples, such as freshly cleaved highly oriented pyrolytic graphite (HOPG) and mica. However, the resolution of AFM for rough samples depends on the morphology and size of the tip and the samples themselves. Several tips were used to assure reproducible AFM images. Generally speaking, sharp tips gave very well-defined step edges, while multiple tips resulted in replicas of surface features, for example identical and parallel steps. The piezoelectric scanners were calibrated against an Au grating, and less than 5% error was possible with low thermal drift. All images were collected in constant-deflection mode, i.e., a feedback loop adjusted the piezoelectric scanner to maintain a constant vertical force between the tip and the sample. The magnitude of the vertical force was in the neighborhood of 10^{-8} N.

Synthesis of Metal(II) Alkanebisphosphonate Powders and Thin Film Preparation. $M_2[O_3P(CH_2)_nPO_3]\cdot 2H_2O$ (M_2-C_nBP, M = Zn, Cu). Metal(II) bisphosphonates are easily formed, because of their low solubility, when bisphosphonic acids are mixed with metal(II) salts in ethanol solution. However, the powders produced by this method were found to be amorphous to X-rays. In order to improve their degree of crystallinity, the powders were precipitated from aqueous hydrochloric acid by slow addition of NaOH solution. Typically, 10 mmol of C_nBPA was dissolved in concentrated HCl (36.5–38.0%), which was added to the bisphosphonic acid until the solution was clear. Aqueous $Zn(ClO_4)_2\cdot 6H_2O$ (25 mmol in 20 mL of H_2O) was added to the stirred acid solution, to which 2 M NaOH was subsequently added dropwise. A white precipitate began to form at pH 1.5. The precipitation was complete at pH 4–5, and the product was filtered, washed with copious amounts of water and ethanol, and then dried in air. Zirconuim 1,10-decanebisphosphonate, Zr-C_{10}BP, was prepared in microcrystalline form from $ZrOCl_2\cdot 8H_2O$ and C_{10}BPA in aqueous HF, according to the method of Alberti et al.[17b] Poorly crystalline Zr-C_{10}BP was prepared by rapid mixing of aqueous solutions containing stoichiometric amounts of $ZrOCl_2\cdot 8H_2O$ and C_{10}-BPA.

Multilayer films of Zn_2-C_nBP were grown on polycrystalline gold substrates using the sequential adsorption scheme outlined in Figure 1. Clean gold substrates were first incubated in the MBPA anchoring agent solution (1 mM in ethanol) as previously described.[13b,20] The phosphonic acid-terminated surface was then immersed alternately in 5 mL of 5 mM $Zn(ClO_4)_2\cdot 6H_2O$ or $Zn(CH_3COO)_2\cdot 2H_2O$ and 5 mM bisphosphonic acid (both in 100% ethanol), each for 10 min, in order to grow the desired number of zinc alkanebisphosphonate layers. The samples were rinsed between adsorption steps by immersing the sample in an ethanol bath (a few milliliters), agitating by hand while holding the sample with tweezers, renewing the ethanol solution, and repeating at least four times. The multilayer films were examined by XPS, which gave observable signals for only Zn, P, O, and C on the surface. Cu_2-C_8BP was prepared under similar conditions (from cupric acetate monohydrate) as both a bulk solid and multilayer thin films. Zr-C_nBP films were grown on gold and silicon substrates at room temperature from aqueous solutions of $ZrOCl_2\cdot 8H_2O$ and C_nBPA as previously described.[13b]

Results and Discussion

Quartz Crystal Microbalance (QCM) Measurements of Film Growth. Mass (Δm) and frequency (Δf) changes for QCM devices

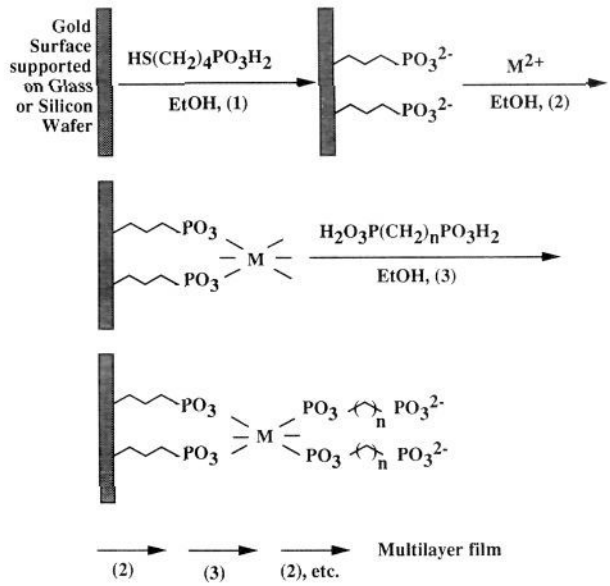

Figure 1. Sequential adsorption scheme for growing zinc bisphosphonates multilayer films on gold surfaces.

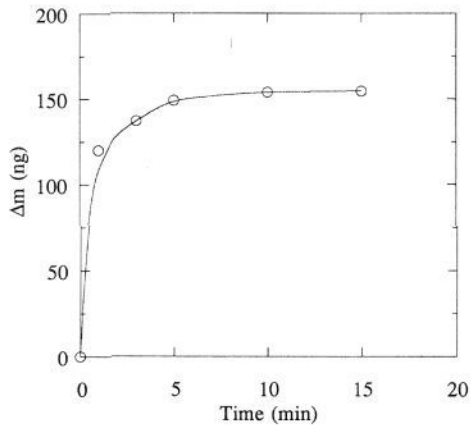

Figure 2. QCM (f_0 = 9 MHz) trace of mass change vs time for formation of a single Zn_2-C_{14}BP layer on a Zn^{2+}-terminated surface.

are related by the Sauerbrey equation (eq 1), in which ρ_q and μ_q are density and shear modulus of quartz (2.65 g/cm^3 and 2.95 × 10^{11} dyn/cm^3, respectively), A is the electrode area, and f_0 is the resonant frequency.

$$\Delta f = \frac{-2\Delta m f_0^2}{A(\rho_q \mu_q)^{1/2}} \qquad (1)$$

Figure 2 shows a trace of mass change vs time for assembly of a C_{14}BPA monolayer on a Zn^{2+}-terminated QCM (resonant frequency 9 MHz) surface. The Zn^{2+}-terminated QCM surface was prepared by immersing an MBPA-modified QCM in a zinc perchlorate solution for approximately 4 h. The total mass deposited by immersion in the zinc-containing solution was 57 ng, which is about twice that expected for monolayer coverage of the apparent (geometrical) surface area of the QCM by $Zn(H_2O)_6^{2+}$. Allowing for the surface roughness factor of 2.0, determined electrochemically, this mass change is consistent with the deposition of a monolayer of Zn^{2+} on the MPBA monolayer. Mass changes due to the adsorption of C_{14}BPA occurred dramatically within the first few minutes and reached a plateau within 10 min. After 15 min, a weight gain of 154 ng was calculated from the frequency change. This is again about twice the theoretical amount (70 ng), based on a molecular surface

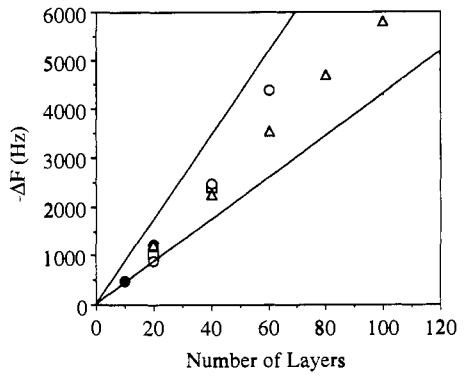

Figure 3. QCM data (f_0 = 6 MHz) for growth of Cu_2-C_8BP multilayer films. Frequency measurements were made after deposition of every 10–20 layers for 20- (●), 40- (□), 60- (○), and 100-layer (△) samples and are compared to frequency changes calculated from eq 1, assuming surface roughness factors of 1.0 and 2.0 (solid lines).

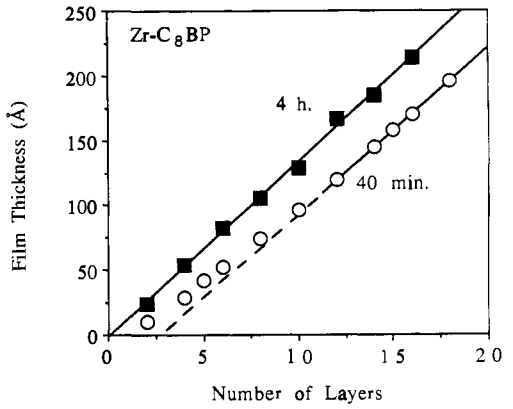

Figure 4. Film thickness vs number of layers for Zr-C_8BP films grown on silicon, using long (4 h) and short (40 min) immersion times. The refractive index of bulk $Zr(O_3P(CH_2)_8PO_3)$, 1.575, was used in the calculation of film thicknesses from ellipsometric data.

area of 27.2 Å^2/molecule[18c] and the apparent area of the 0.159 × 2 cm^2 electrode. As with the Zn^{2+} adsorption step, this result is consistent with deposition of a single monolayer on the roughened gold surface.

Figure 3 shows QCM results for the growth of 20-, 40-, 60-, and 100-layer Cu_2-C_8BP films, prepared using 10-min adsorption steps. In this case the mass change per layer for all samples is intermediate between that calculated theoretically on the basis of the electrochemically measured surface area of the bare gold substrate (roughness factor = 2.0). This result is consistent with some smoothing of surface roughness by thick multilayer films. AFM images of multilayers on rough gold surfaces (vide infra) provide direct evidence for this surface-smoothing effect.

The time course of these adsorption reactions is striking in the sense that monolayer growth appears to be substantially complete within 10 min of exposure to the alkanebisphosphonic acid solution. While phosphonates also adsorb rapidly on Zr^{4+}-terminated surfaces,[13a] much longer exposure times (on the order of hours at room temperature) are required in order to achieve compact monolayers that form well-ordered multilayer films. This point is illustrated in Figure 4, which compares ellipsometric data for growth of Zr-C_8BP multilayer films using long (4 h) and short (40 min) immersion times. With long immersion, the change in thickness with each new layer is constant, and corresponds well to the bulk solid (13.4 Å, compared to 13.58 Å for bulk Zr-$(O_3P(CH_2)_8PO_3)$). With short immersion times, the films are much thinner than expected from the XRD layer spacing. After ca. 10 layers have been deposited, the increase in thickness with each adsorption step becomes constant, but is only 12.8 Å/layer. In contrast, very short adsorption times under mild conditions appear to be adequate for the formation of good divalent metal phosphonate multilayers.

Table I. XPS Data: Binding Energies (BE, ±0.2 eV) and Peak Areas (Arbitrary Units) for Eight-Layer Phosphonate- and Zinc-Terminated Zn_2-C_{12}BP Films on Gold[a]

	PO_3^{2-}-terminated			Zn^{2+}-terminated		
	BE	area	A_{norm}	BE	area	A_{norm}
Zn	1025.2	386	.040	1025.9	94	.064
P	135.5	48	.075	136.3	6.5	.093
O	533.8	287	.215	534.1	38	.176
C	287.0	296	.670	287.7	47	.667

	$A_{norm(Zn)}/A_{norm(P)}$	$A_{norm(Zn)}/A_{norm(P)}$
obs	0.53	0.69
calc, small λ's	0.10	1.14
calc, large λ's	0.51	0.68

[a] A_{norm} represents normalized peak area/atomic sensitivity factor.

One factor contributing to the difference in film growth kinetics is the relative solubility of the divalent and tetravalent metal phosphonate salts. Because the latter are much less soluble, the growth of crystalline domains and elimination of defects via Ostwald ripening are expected to be slower. Another factor may be the choice of solvents (water in the case of the Zr^{4+} films vs ethanol for Zn^{2+} and Cu^{2+}), since it is likely that the state of aggregation and the conformation of the amphiphilic phosphonic acids will be different in the two solvents. In either case it is likely that a poorly ordered, incomplete monolayer of bisphosphonic acid adsorbs immediately on the metal ion-terminated surface. The annealing of this layer, over a much longer time scale, into a well-ordered one requires the breaking and reformation of metal–phosphonate linkages. This process will have a higher activation barrier in the case of the tetravalent compounds. Consistent with this model, Katz and co-workers have found that the quality of zirconium phosphonate multilayer films can be improved significantly by employing nonaqueous solvents and higher adsorption temperatures.[15]

X-ray Photoelectron Spectroscopy. Table I shows XPS data for an eight-layer film of Zn_2-C_{12}BP grown on gold. The core-orbital binding energies were corrected by referencing the aliphatic C_{1s} peak to 285.0 eV.[25] At the detection limit of the technique, there is no evidence for incorporation of perchlorate counterions. The normalized peak areas were calculated from eq 2, where ASF is an empirically determined atomic sensitivity factor,[26] and the summation is carried out over the n different elements detected.

$$A_{norm} = \frac{\text{area/ASF}}{\sum_{j=1}^{n}(\text{area}_j/\text{ASF}_j)} \qquad (2)$$

Although the ratio of Zn to P atoms in the films is essentially unity, the apparent ratio (i.e., the ratio of the A_{norm} values) is lower because the two elements have different photoelectron escape depths. Figure 5 shows, schematically, the structure of a phosphonate-terminated film. Such a film contains the elements of interest, each with a characteristic photoelectron mean free path (λ), at a variety of depths. For a given element at a certain depth (d) in the film, the contribution to the measured XPS peak intensity is given by eq 3.[27] where I_0 is the intensity obtained for

$$I = I_0 e^{-d/\lambda} \qquad (3)$$

the same element at the outer edge of the film. In order to calculate

(25) Beamson, G.; Briggs, D. *High Resolution XPS of Organic Polymers*; John Wiley & Sons: Chichester, England, 1992; Section 6.3, p 26.
(26) VGS 1000 manual, VG Scientific Ltd.: East Grinstead, UK, 1983.
(27) Ertl, G.; Kuppers, J. *Low Energy Electrons and Surface Chemistry*, 2nd ed.; VCH: Weinheim, FRG, 1985; pp 74–79.

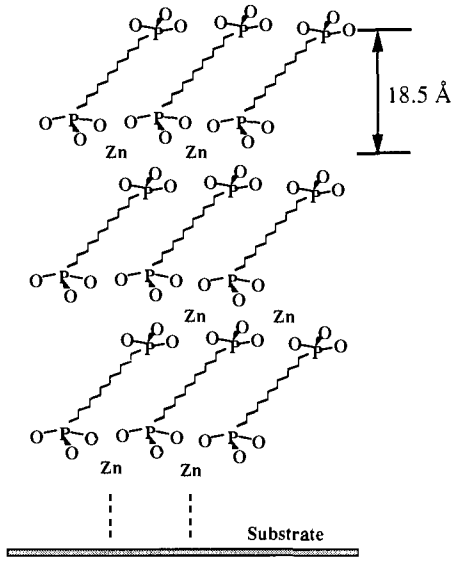

Figure 5. Structural model for a phosphonate-terminated film, used to calculate XPS A_{norm} values (see text).

the ratio of A_{norm} values for Zn and P, these contributions must be summed over the entire structure, i.e.,

$$\frac{A_{norm(Zn)}}{A_{norm(P)}} = \frac{m_{Zn} \sum_{Zn\ atoms} e^{-d_{Zn}/\lambda_{Zn}}}{m_P \sum_{P\ atoms} e^{-d_P/\lambda_P}} \quad (4)$$

In eq 4 the summation is carried out over the eight layers of the film, and m represents the multiplicity of atoms at a given depth ($m_{Zn} = 2$; $m_P = 1$). The d values are easily calculated from the structure model, but the λ values depend on the nature of the material from which the photoelectrons are generated. Typical λ_{Zn} and λ_P values are dense materials such as metals and metal oxides are 7.5 and 17.0 Å, respectively.[25] Using these values, one obtains very poor agreement (Table I) between observed and calculated XPS intensity ratios. In particular, the Zn signal from the phosphonate-terminated films is much stronger than that expected on the basis of a λ_{Zn} value smaller than the layer thickness.

Previous XPS experiments with Langmuir–Blodgett films and self-assembled multilayers have shown anomalously large photoelectron mean free paths, presumably because of "channeling" of photoelectrons along the alkyl chains.[13d] Because the latter are held together weakly by van der Waals forces, there are directions in the film in which the photoelectron mean free path is long. Keeping the ratio of λ_{Zn} to λ_P constant, but multiplying both by a large factor, we find substantially better agreement with the observed XPS intensities. The A_{norm} ratios shown in Table I were calculated with λ_{Zn}, λ_P = 60, 136 Å, a factor of 8 larger than the λ values normally used for dense isotropic materials. In this case excellent agreement is obtained for both the phosphonate- and zinc-terminated films. Larger λ values gave poorer agreement with the observed ratios; in particular, as λ_{Zn} is increased, the calculated ratio approaches unity, as expected. These results are consistent with the structural model shown in Figure 5, and with a stoichiometry matching that of the bulk material, $Zn_2[O_3P(CH_2)_{12}PO_3]\cdot 2H_2O$, for the adsorbed multilayers.

Structural Characterization by Ellipsometry and X-ray Diffraction. Figure 6 shows plots of film thickness, determined by ellipsometry, vs number of layers for multilayer films of Zn_2-C_nBP (n = 8, 10, 12, 14). The slopes of the lines in Figure 6 give average increments in layer thickness of 14.5, 16.4, 18.6, and 20.5 Å for n = 8, 10, 12, and 14, respectively. Much of the

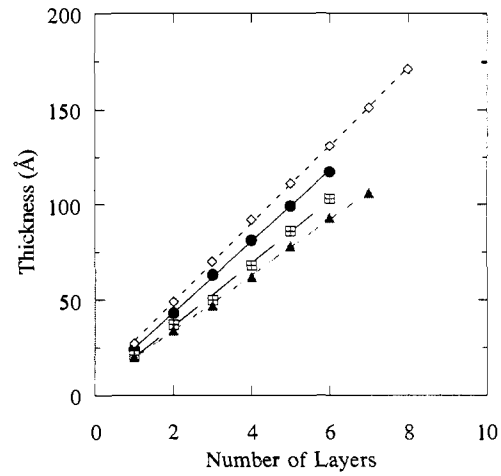

Figure 6. Ellipsometric film thickness vs number of layers for Zn_2-C_nBP thin films: n = 14 (◇), 12 (●), 10 (□), and 8 (▲).

Table II. X-ray Powder Diffraction Data for $Zn_2[O_3P(CH_2)_4PO_3]\cdot 2H_2O$[a]

d_{obs}, Å	d_{calc}, Å	hkl	I_{rel}	d_{obs}, Å	d_{calc}, Å	hkl	I_{rel}
9.697	9.710	010	100	2.702	2.704	031	20
4.854	4.855	020	16	2.397	2.399	211	18
4.251	4.389	011	22	2.383	2.385	012	20
3.844	3.733	101	8	2.233	2.235	140	17
3.641	3.704	120	11	2.038	2.035	141	16
3.410	3.456	021	13	1.948	1.942	050	8
3.176	3.236	030	28	1.817	1.806	051	19
2.915	2.959	121	12	1.752	1.751	311	13

[a] Orthorhombic, $Pmn2_1$, or monoclinic, Pn; a = 5.732 Å, b = 9.711 Å, c = 4.921 Å, $\beta \approx 90°$.

±1.0-Å uncertainty in these results originates in factors such as the gold surface roughness, the accuracy of the ellipsometric method,[28] and the estimated refractive index. For short alkyl chains ($n \leq 10$), zinc acetate solutions were used, and zinc perchlorate was used for longer alkyl chains. Use of the perchlorate salt for n = 10 gave a slope of ca. 7.5 Å/layer, indicating the formation of porous or patchy films. It is possible that the slight solubility of films prepared from perchlorate solutions results in incomplete layer growth or dissolution of the film in ethanol during the rinsing steps. This solubility could arise from ion-pairing or coordination of perchlorate to Zn^{2+}; however, chlorine was not detected in XPS spectra of ethanol-rinsed films.

X-ray powder diffraction patterns of polycrystalline Zn_2-C_nBP solids were indexed using in-plane cell constants from the model structure $Fe(O_3PC_2H_5)\cdot H_2O$[18k] (space group Pn). Table II lists X-ray diffraction data for $Zn_2C_4BP\cdot 2H_2O$. Interlayer spacings for $n > 4$ were determined by averaging the d-spacings of the ($0k0$) reflections, where k = 1–3. Averge layer distances in the thin films, determined by ellipsometry, are compared with those of the bulk solids in Figure 7. X-ray powder diffraction gave layer spacings of 9.70, 14.0, 16.30, 18.30, and 20.40 Å/layer for n = 4, 8, 10, 12, and 14, respectively, in essentially perfect agreement with the ellipsometric results for Zn_2-C_nBP films. An increment of 1.07 Å per CH_2 group can be calculated from these layer spacings. Projecting the carbon–carbon bond (length 1.540 Å) onto the axis of an ideal all-trans CH_2 chain results in a spacing of 1.256 Å per CH_2.[29] The observed increment of 1.07 Å per CH_2 indicates that alkyl chains in the zinc phosphonate salts and multilayer films are tilted 31° away from the surface normal. The average layer thickness of Cu_2-C_8BP multilayer films, obtained by ellipsometry, was 14.9 Å, again in good

(28) Azzam, R. M. A.; Bashara, N. M. *Ellipsometry and Polarized Light*; North-Holland Publishing Company: Amsterdam, 1997.
(29) Fromherz, P.; Oelschlägel, U.; Wilke, W. *Thin Solid Films* **1988**, *159*, 421.

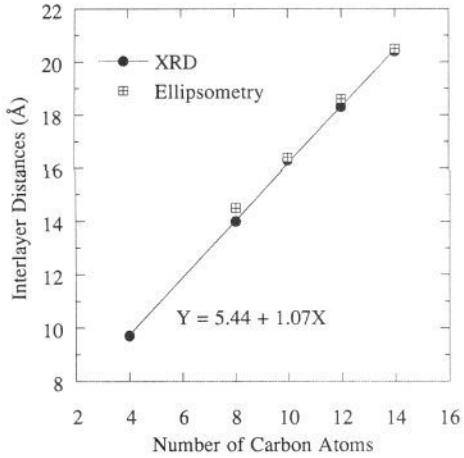

Figure 7. Comparison of powder XRD and average ellipsometric interlayer distances vs number of carbon atoms for Zn_2-C_nBP.

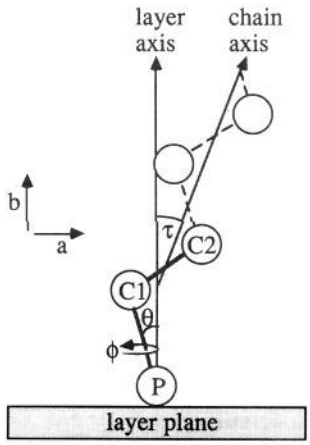

Figure 8. Schematic representation of $Fe(O_3PC_2H_5)\cdot H_2O$ and related divalent metal phosphonate structures. The alkyl chain tilt angle τ is calculated from θ and from the chain twist angle ϕ. The crystallographic a axis in $Fe(O_3PC_2H_5)\cdot H_2O$ (space group Pn) corresponds to the c axis in $M(O_3PC_6H_5)\cdot H_2O$, M = Mn, Zn (space group $Pmn2_1$).

agreement with X-ray powder diffraction results for the corresponding bulk solid (14.3 Å).

The observed alkyl chain tilt angle in Zn_2-C_nBP may be compared with that expected from the crystal structure of $Fe(O_3PC_2H_5)\cdot H_2O$, which has recently been determined by Bujoli et al.[18k] These relevant angles in the $M^{II}(O_3PR)\cdot H_2O$ structures are shown in Figure 8. Assuming that the alkyl chain prefers in all-trans configuration, the chain tilt angle τ is determined by the angle θ between the P–C1 bond and the stacking axis and by the twist angle ϕ. The $Fe(O_3PC_2H_5)\cdot H_2O$ structure is quite similar to that of $Mn(O_3PPh)\cdot H_2O$[18c] and $Zn(O_3PPh)\cdot H_2O$,[18e] except that in the latter a crystallographic mirror plane constrains ϕ to be 0 or 180°. Weak superlattice diffraction spots indicate, however, that the true crystal symmetry of the benzenephosphonates is probably monoclinic[18c] and that the phenyl rings are staggered with respect to the (apparent) mirror plane. From the coordinates of atoms in the monoclinic $Fe(O_3PC_2H_5)\cdot H_2O$ structure we calculate θ = 14, ϕ = 57°; the alkyl groups are staggered along the crystallographic a axis, removing the c-axis mirror plane and permitting more efficient chain packing. The alkyl chain axis, defined as the line joining the midpoints of the P–Cl and C1–C2 bonds, is tilted by τ = 34° from the crystallographic b (stacking) axis in $Fe(O_3PC_2H_5)\cdot H_2O$, in excellent agreement with the 31° value obtained from X-ray and ellipsometric measurements of Zn_2-C_nBP bulk solids and thin films.

Table III. IR Peak Assignments (cm^{-1}) for $Zn_2[O_3P(CH_2)_8PO_3]\cdot 2H_2O$

modes	bulk	film	modes	bulk	film
H_2O	3452			1187	
	2941			1151	
$\nu_{as}(CH_2)$	2923	2927	$\nu_{as}(PO_3)$		1125
	2909				1092 (shoulder)
$\nu_s(CH_2)$	2848	2853		1084	
H_2O	1627	1639		1067	
CH_2 def bending	1467	1467	$\nu_s(PO_3)$	1010	
CH_2 def scissor	1412	1410		977	
CH_2 wag	1255				941
		1236		927	

Table IV. Peak Positions (cm^{-1}) of the CH_2 Stretching and Water Vibrations for Bulk $Zn_2[O_3P(CH_2)_nPO_3]\cdot 2H_2O$[a]

	C_4	C_8	C_{10}	C_{12}	C_{14}
CH_2	2866	2848	2848	2848	2848
	2903	2909	2916		
	2931	2923	2921	2917	2918
	2946	2941			
H_2O	1630	1627	1627	1627(w)	
	3462	3452	3437	3430	

[a] Blanks indicate absence of peaks.

The close agreement of the film and bulk layer spacings, together with the mass changes detected by QCM, provides strong evidence that the Zn and Cu multilayer films are packed at approximately the same alkyl chain density, and probably in the same molecular arrangement, as are microcrystals of the bulk solids.

Infrared Spectra. Table III lists the mid-IR absorption bands of bulk Zn_2-C_8BP in a KBr pellet and those of multilayer thin films on gold. In both spectra, bands between 970 and 1150 cm^{-1} are attributed to P–O stretching vibrations, by analogy to assignments previously made for $Mg(O_3PC_{12}H_{25})\cdot H_2O$.[18d] The OH stretching vibration of the POH group at 2700–2500 and 2350–2100 cm^{-1} does not appear, indicating complete conversion of the phosphonic acid to the zinc salt. The Zn–O stretching vibration lies at low frequency, beyond the range of the detector used. Peak positions in the spectra of bulk Zn_2-C_nBP depend on the length of the alkyl chain. For example, the antisymmetric CH_2 stretching frequencies are 2931, 2923, 2921, 2917, and 2918 cm^{-1} for n = 4, 8, 10, 12, and 14, respectively. There are also two unassigned bands in the spectra of the isotropic bulk solids, possibly combination or overtone bands of the CH_2 deformations, at 2903 and 2946 cm^{-1} for n = 4–10. These bands are not observed for n = 12 and 14 or in any of the thin film samples. The water vibrational frequencies decrease with increasing alkyl chain length, as do the peak intensities. For n = 14, water vibrations are not observed. Table IV shows trends in the CH_2 stretching and the water stretching and bending frequencies for bulk Zn_2-C_nBP. The frequency shifts are due to the van der Waals forces between chains, which grow progressively stronger as the chains become longer. In the case of Cu_2-C_8BP, the antisymmetric and symmetric CH_2 stretching bands are found at 2918 and 2849 cm^{-1}, an unassigned band at 2935 cm^{-1}, and the water vibration at 3347 cm^{-1}.

Figure 9 compares the reflection IR spectra for one- to six-layer Zn_2-C_8BP films to the bulk spectrum. In the multilayer spectra, which are similar to those of the isotropic powder, the $\nu_{as,s}(CH_2)$ and P–O stretching bands dominate the spectra, and the hydrate bands are not observable. A plot (inset in Figure 9) of integrated peak area vs number of layers is linear for all three bands, supporting the idea of stepwise layer growth of the films.

The differences between film and bulk IR spectra for Zn_2-C_8BP may be interpreted in terms of structural insights gained from XRD and ellipsometric measurements. For the reflectance (thin film) spectra, the intensity of a given band depends on the

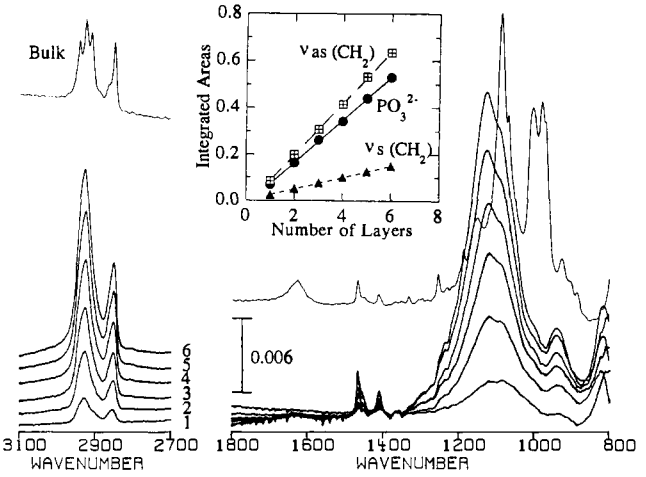

Figure 9. Reflection absorption IR spectra for Zn_2-C_8BP thin films (one to six monolayers). The isotropic bulk spectrum is also shown (thin line); the vertical bar scale corresponds to the thin films. Inset: integrated peak areas vs number of layers; area under the PO_3^{2-} peaks is scaled by $^1/_{10}$.

direction of the dipole moment change relative to the surface normal.[30] The relative intensity is governed by the surface selection rule, which states that modes that have a large component of their dipole moment change in the plane of the gold will be attenuated. Qualitative comparison of the C–H and P–O stretching bands shows that the former are enhanced relative to the latter in going from the isotropic sample to the thin multilayer film. This is consistent with the observed tilt (31°) and twist (50–60°) angles expected from the structural model shown in Figure 8. The CH_2 planes are perpendicular to the chain axis and therefore make an angle of 59° to the surface normal. This implies that the dipole moment changes occur at approximately 59 and 78°, respectively, for the symmetric and antisymmetric C–H stretching modes. The antisymmetric PO_3 stretching mode, on the other hand, should be polarized nearly in the plane of the gold surface, consistent with somewhat lower relative intensity of bands in the P–O stretching region. The absence of a band at about 3450 cm^{-1} indicates that the OH stretching vibration is also polarized roughly parallel to the surface. Unfortunately, bands in the P–O stretching region of the IR spectra are not well-resolved, making detailed mode assignments and quantitative comparisons of band intensity with structural models difficult.

Another important piece of information concerning alkyl chain conformation is provided by the frequencies of the $\nu_{as,s}(CH_2)$ stretching modes. These frequencies have been used to differentiate between all-trans (crystalline) and disordered (liquid-like) conformations of alkyl chains.[5c,30a] In general, these frequencies increase by about 5–10 cm^{-1} in going from a crystalline all-trans to a disordered (gauche-rich) conformation. Table V lists results of peak positions and widths for both the bulk solid and multilayer thin films of Zn_2-C_nBP (one to five monolayers). In the case of both Zn_2-C_8BP and Zn_2-C_{14}BP, the $\nu_{as,s}(CH_2)$ frequencies increase by 4 cm^{-1} in going from the polycrystalline bulk solid to the multilayer film.

Because the collective van der Waals forces between chains increase with increasing chain length, the degree of order of a monolayer film increases as the number of methylene groups increases.[5c,30] Comparison of peak widths for different chain lengths in the Zn_2-C_nBP series shows that this trend also holds in the present case. Table V summarizes the peak widths of the $\nu_{as,s}(CH_2)$ vibrations for both bulk and thin film Zn_2-C_nBP. Multilayer films of Zn_2-C_8BP have a liquid-like structure (peak widths 15–20 cm^{-1} larger than those of the crystalline bulk compound), in contrast to Zn_2-C_{14}BP, which shows negligible differences in peak widths compared to the bulk phase. Since Zn_2-C_{14}BP films have narrow peak widths but give shifts of 4 cm^{-1} in CH_2 stretching frequencies, they might be described as "fairly" ordered, but still not equivalent to the bulk crystalline layered solid. An important observation, obtained by subtracting sequential layer spectra, is that neither the peak positions nor their widths change as new layers of Zn_2-C_nBP are added. This result shows that each new layer has the same degree of crystallinity as the one it is deposited on.

Multilayer films of Cu_2-C_8BP also show a liquid-like structure, with somewhat smaller peak widths but larger peak position shifts for the CH_2 stretching vibrations relative to Zn_2-C_8BP (Table V). The anomalously small peak width obtained for the first monolayer in this case may be an artifact of poor signal to noise in the spectrum of a single layer.

Table V also compares peak widths for layers of the tetravalent metal phosphonate $Zr[O_3P(CH_2)_{10}PO_3]$ (Zr-C_{10}BP) with the M_2-C_8BP compounds. Despite the fact that Zr-C_{10}BP has a slightly longer alkyl chain and 2–4 h was allowed for adsorption of each layer, peak widths for the CH_2 stretching vibrations are roughly comparable to those of M_2-C_8BP and also indicate a liquid-like structure. In the case of Zr-C_{10}BP, the bulk solid may be prepared in well-crystallized form from aqueous HF solution[17b] or in poorly crystalline form by rapidly mixing zirconyl chloride and C_{10}-BPA solutions. Infrared peak widths for the crystalline material are comparable to those of the bulk M_2-C_nBP salts, indicating well-packed alkyl chains. The rapidly precipitated material, however, gives very broad X-ray diffraction peaks, indicative of very small (50–100 Å) ordered domains. The infrared spectrum of this material also shows very broad CH_2 stretching peaks at relatively high frequency. This result may be understood in terms of the size of crystalline domains within the bulk solids and thin films; that is, the domain size in films of M_2-C_8BP and Zr-C_{10}BP is intermediate between that of the poorly and highly crystalline bulk solids, the latter possessing ordered domains of 500 Å or more, judging from the width of X-ray diffraction lines. On the other hand, Zn_2-C_{14}BP films resemble the well-crystallized bulk material. These results parallel those found with self-assembling amphiphiles, where short alkanethiol[5c] ($<C_8$) and *n*-alkanoic acids[30a] ($<C_{12}$) give monolayers showing liquid-like IR spectra, variable ellipsometric thickness, and anomalously low contact angles, whereas longer alkyl chains result in monolayers possessing large crystalline domains. For an equivalent alkyl chain length, the divalent metal phosphonate films appear to be less well-ordered than *n*-alkanethiol monolayers on gold. For example, the frequency of the $\nu_{as}(CH_2)$ mode, which is most sensitive to chain order, shifts to 2919 and 2921 cm^{-1}, respectively, in going from the crystalline state (2918 cm^{-1}) to a monolayer film for CH_3-$(CH_2)_n$SH, n = 11, 7.[5a] In contrast, the Zn-C_nBP (n = 8, 14) films give peaks at 2927 and 2922 cm^{-1}, respectively.

Atomic Force Microscopy Imaging. Figure 10 shows AFM images of a bare Au substrate and of Zn^{2+}-terminated Zn_2-C_{12}-BP multilayer films (13 monolayers, ca. 24 nm thick) on the Au surface. The main features of both samples are 1-μm-wide islands with 2–5-nm corrugation. Deposition of the bisphosphonate film does not result in drastic morphology changes in the Au surface, except that the feature size appears larger, consistent with some smoothing of surface corrugation. This is reasonable, in that deposition of a uniform thin film is expected to follow the substrate surface morphology. Furthermore, retention of the original morphology on this scale implies that the surface film has been built up uniformly so that no patches or islands of film are discerned by AFM, at least within the 15-μm area scanned. Imaging of five different areas gave similar results.

(30) (a) Allara, D. L.; Nuzzo, R. G. *Langmuir* **1985**, *1*, 45. (b) *Ibid.* **1985**, *1*, 52.

(31) (a) Synder, R. G.; Strauss, H. L. *J. Phys. Chem.* **1982**, *86*, 5145. (b) Synder, R. G.; Maroncelli, M.; Strauss, H. L.; Hallmark, V. M. *J. Phys. Chem.* **1986**, *90*, 5623. (c) Scheuing, D. R. *Fourier Transform Infrared Spectroscopy in Colloid and Interface Science*; ACS Symposium Series 447, American Chemical Society: Washington, DC, 1991.

Table V. Peak Widths (cm^{-1}) for Zn_2-C_8BP, Cu_2-C_8BP, Zn_2-C_{14}BP, and Zr-C_{10}BP Films on Gold[a]

	Zn_2-C_8BP		Cu_2-C_8BP		Zn_2-C_{14}BP		Zr-C_{10}BP	
no. of layers	2927 cm^{-1}	2853 cm^{-1}	2927 cm^{-1}	2856 cm^{-1}	2922 cm^{-1}	2852 cm^{-1}	2929 cm^{-1}	2854 cm^{-1}
1	40.8 (2930)	26.7 (2856)	29.5	23.6	24.8	16.5	41.1	25.1
2	40.8	26.7	37.8	26.0	24.2	15.9	41.1	23.4
3	40.8	26.4	36.6	24.2	24.2	14.8	41.1	23.0
4	40.8	26.7	34.8	26.0	24.4	14.2	41.1	23.4
5	40.8	26.7	34.8	26.0	24.2	13.6		
6	40.8	26.7	36.0	27.2				
bulk	20.7 (2923)	11.6 (2848)	24.8 (2918)	17.7 (2848)	29.5 (2918)	13.6 (2848)	26.6 (2922) (crystalline)	11.8 (2848)
							55.4 (2931) (poorly crystalline)	23.7 (2856)

[a] Peak positions for bulk and first layer are indicated in parentheses.

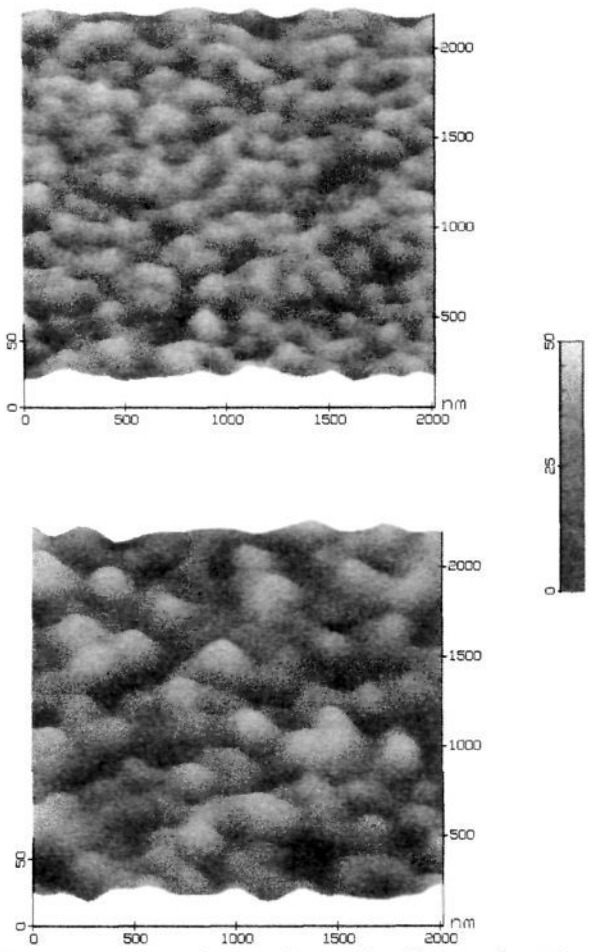

Figure 10. AFM images for (a, top) bare gold and (b, bottom) a 13-layer Zn^{2+}-terminated Zn_2-C_{12}BP film in a 2 × 2 μm area.

AFM also provided a rough measure of film thickness. After the scan length was decreased from 15 to 5 μm and the tip-to-surface force was increased to ca. 10^{-7} N, a 5-μm depression was made by the tip in the course of a 5-min scan. The AFM revealed an average corrugation of 22 ± 3 nm due to the depression (Figure 11). This result is consistent with the ellipsometry data. Nevertheless, it is somewhat peculiar that no material piled up along the edge of the depression, as one might expect. It is possible that the material removed was transferred to the tip without degrading the resolution of the AFM seriously and/or the tip caused inelastic deformation of the film. Similar explanations have been previously applied to AFM etching of organic films.[32] Interestingly, the depth of the depression was proportional to imaging time at the beginning of the experiment, but after 5 min it became constant at ca. 22 nm. Finally, it is important to note that this force-induced etching did not create similar depressions on a bare Au surface. In control experiments carried out with unmodified Au, no change of the surface morphology was discerned by the AFM under conditions that caused depressions in the bisphosphonate film.

(32) (a) Gratz, A. J.; Manne, S.; Hansma, P. K. *Science* **1991**, *251*, 1343. (b) Delawski, E.; Parkinson, B. A. *J. Am. Chem. Soc.* **1992**, *114*, 1661.

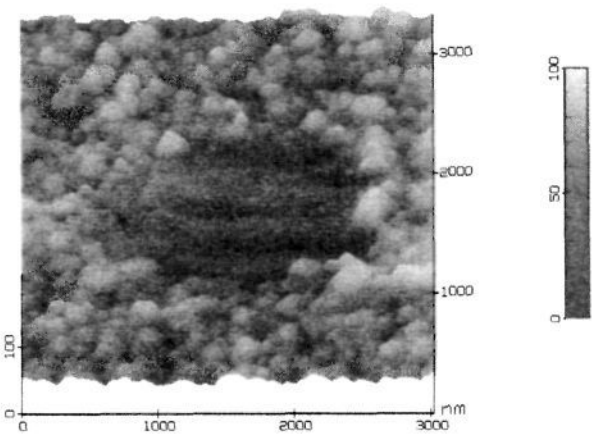

Figure 11. AFM image for a Zn^{2+}-terminated Zn_2-C_{12}BP film in a 3 × 3 μm area. The depression area (1 × 1 μm) made by the AFM tip shows an average corrugation of 22 ± 3 nm (see text).

Summary and Conclusions

Salts of divalent metal (Zn and Cu) phosphonates grow as well-ordered multilayer films by sequential adsorption of soluble perchlorate or acetate salts and alkanebisphosphonic acids from ethanol. These materials present an attractive alternative to the analogous zirconium salts, because thick films (at least 100 layers) may be grown at room temperature in a relatively short period of time. Surface-sensitive probes show that the structural integrity of these films is better than that of the zirconium analogues, consistent with the higher solubility and greater tendency to crystallize of the Cu and Zn compounds. Finally, we note that these compounds in bulk form are known to undergo shape-selective intercalation reactions. This property suggests the possibility of making thin film sensors based on their intercalation reactions, as well as new opportunities for structurally tailoring surface films by intercalating molecules of interest. These ideas will be explored in future experiments.

Acknowledgment. We thank Prof. Eugene Smotkin for supplying the design of the oscillator circuit and for helpful advice with the QCM experiments. This work was supported by grants from the National Science Foundation (CHE-9217719) and the Robert A. Welch Foundation (F-1034). T.E.M. also thanks the Camille and Henry Dreyfus Foundation for support in the form of a Teacher-Scholar Award.